

Graphene on transition-metal dichalcogenides: a platform for proximity spin-orbit physics and optospintronics

Martin Gmitra and Jaroslav Fabian

*Institute for Theoretical Physics, University of Regensburg,
93040 Regensburg, Germany*

Hybrids of graphene and two dimensional transition metal dichalcogenides (TMDC) have the potential to bring graphene spintronics to the next level. As we show here by performing first-principles calculations of graphene on monolayer MoS₂, there are several advantages of such hybrids over pristine graphene. First, Dirac electrons in graphene exhibit a giant global proximity spin-orbit coupling, without compromising the semimetallic character of the whole system at zero field. Remarkably, these spin-orbit effects can be very accurately described by a simple effective Hamiltonian. Second, the Fermi level can be tuned by a transverse electric field to cross the MoS₂ conduction band, creating a system of coupled massive and massless electron gases. Both charge and spin transport in such systems should be unique. Finally, we propose to use graphene/TMDC structures as a platform for optospintronics, in particular for optical spin injection into graphene and for studying spin transfer between TMDC and graphene.

Graphene spintronics [1] has relied exclusively on electrical spin injection [2–4]. Combining graphene with semiconducting two-dimensional TMDC [5] can open new venues for spintronics applications [6, 7]. Indeed, TMDC are becoming increasingly popular in optoelectronics as sensitive photodetectors [8] or, forming lateral heterostructures [9, 10], as two-dimensional solar cells [11]. Important, TMDC have a sizeable spin-orbit coupling and lack space inversion symmetry. As a result, their band structure [12] allows for a valley resolved optical spin excitation by circularly polarized light [13–15]. TMDC can thus facilitate optical spin injection into graphene, in hybrid structures.

Efficient growth of MoS₂ on graphene has already been demonstrated [16–18]. It was reported that graphene on MoS₂ is ultraflat, having large mean free paths [19]; angle-resolved photoemission found an intact Dirac point but a strong hybridization elsewhere in the π system [20]. Technological potentials for these hybrid structures are already being discussed [21], mainly as a basis for non-volatile memory [22], sensitive photodetection [23], and gate-tunable persistent photoconductivity [24]. Recently, the spin Hall effect in graphene on few-layer WS₂ was observed at room temperature [25].

In this paper we establish by first-principles calculations fundamental electronic properties and the spin-orbit fine structure of the graphene Dirac bands for graphene on monolayer MoS₂, and introduce an effective spin-orbit Hamiltonian which explains the proximity induced spin splittings of the Dirac states. We show that the induced spin-orbit coupling is giant, being 20 times more than in pristine graphene. We also discuss the field effect on the band offsets of the two materials. Finally, we present possible experimental schemes to perform optical spin injection into graphene and study spin tunneling from TMDC through graphene.

First-principles results. To establish the electronic and spin properties of graphene on MoS₂ we used first-principles methods based on density-functional theory [26], see Methods. To reduce structural strain we constructed a large supercell of 59 atoms, comprising a 3×3 supercell of MoS₂ and a 4×4 supercell of graphene, with the residual lattice mismatch of 1.4%. The relaxed inter-layer distance between graphene and MoS₂ is 3.37 Å, see Fig. 1a). In this supercell the K point of MoS₂ is mapped to the Γ point in the reduced Brillouin zone. The calculated electronic band structure is shown in Fig. 1b). The Dirac cones of graphene are nicely preserved, with the projected Dirac point (which is also the Fermi level) being slightly below the conduction band edge of MoS₂. The closeness of the Dirac point to the conduction band of MoS₂ enhances screening, which can substantially increase the mean free path in the graphene layer, as recently shown experimentally [19].

The band offsets between graphene and MoS₂ can be controlled by an external electric field applied transverse to the layers. This is demonstrated by our first-principles calculations in Fig. 2a), where we present Δ_c , the difference between the conduction band minima of MoS₂ and graphene. At negative fields (pointing towards MoS₂) the offset increases, leaving both layers neutral. However, positive fields shift the Dirac point above the conduction band minimum of MoS₂ and populate graphene with holes and MoS₂ with electrons. The Fermi level crosses both the valence band of graphene and the conduction band of MoS₂, see Fig. 2b) and c). This field effect can establish a unique system in which massless Dirac electrons are coupled with a conventional 2d electron gas [27].

We now zoom in on the Dirac point at K to see how the electronic spectrum of graphene deforms in the presence of MoS₂. This fine structure is shown in the inset to Fig. 1b). There are two important effects: First, an or-

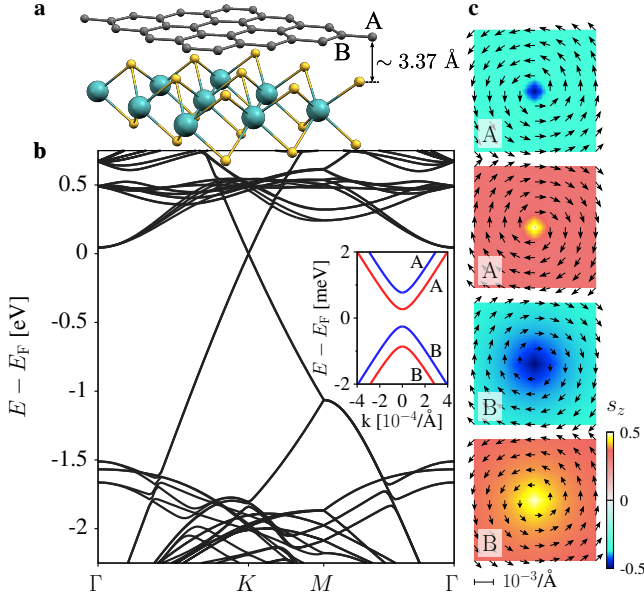


FIG. 1: Calculated electronic and spin properties of graphene on two-dimensional MoS₂. (a) The supercell used in first-principles calculations. (b) Calculated band structure along high symmetry lines. The inset is a zoom to the fine structure of the low energy bands at the Fermi level, around the Dirac point. Bands with positive (negative) z component of the spin are shown in red (blue). The sublattice character (A and B) is also indicated. (c) Spin textures for the four bands of the inset in (b).

bital band gap opens, due to the breaking of the graphene pseudospin symmetry. On average, atoms A and B in the graphene supercell see a different environment coming from the MoS₂ layer. This orbital gap is there even in the absence of spin-orbit coupling. It arises from the effective staggered potential induced by the pseudospin symmetry breaking. Second, spin-orbit coupling combined with the broken space inversion symmetry lifts the spin degeneracy of the Dirac valence and conduction bands and leads to the appearance of four distinct bands. This splitting is on the meV scale, which is giant when compared to the $24 \mu\text{eV}$ spin-orbit splitting in pristine graphene [28]. The inset also shows the orbital character of the bands at K : while the valence states are formed at the B sublattice, the conduction states live on A . The same orbital ordering is at K' .

Another important characteristic of the Dirac states is their spin texture. This is plotted in Fig. 1c) for the four bands from the inset of Fig. 1b). Directly at K the spins are pointing out of the graphene plane, alternating up and down. Increasing the momentum away from K , the spins acquire a winding in-plane component, either clockwise or counterclockwise, suggestive of the strong Rashba effect. At K' the spins are reversed.

Effective Hamiltonian. Can we understand these proximity-induced changes in graphene's band structure

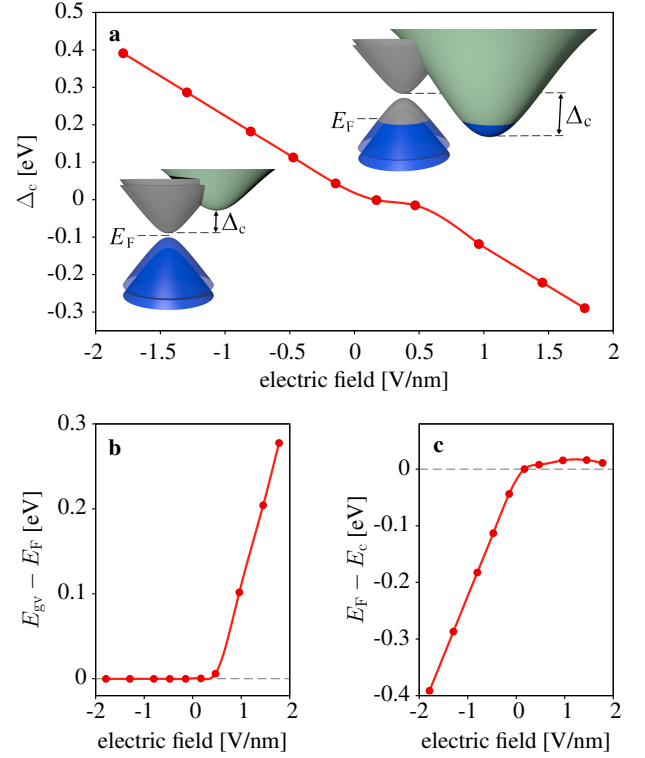


FIG. 2: Field effect on graphene/MoS₂. (a), Calculated offset Δ_c from the conduction band minimum of MoS₂ to graphene, as a function of an applied transverse electric field. At positive fields electrons are transferred from graphene to MoS₂, establishing a massless-massive electrons bilayer. (b) Net Fermi energy for graphene, as the difference of the valence band maximum E_{gv} of graphene and the system Fermi level, E_F . At positive fields the valence band of graphene becomes populated. (c) Net Fermi energy for MoS₂, as the difference between the system Fermi level, E_F , and the conduction band minimum, E_c of MoS₂. The conduction band of MoS₂ becomes populated at positive field, reflecting the population of holes in graphene in (b) as the whole system is neutral.

from an effective model? The answer is not obvious since not only sublattices A and B differ, but even the sites that belong to the same sublattice see different local environments in the supercell. Surprisingly, an effective symmetry-based Hamiltonian with graphene orbitals in the presence of pseudospin inversion symmetry breaking gives a remarkably good description. The model builds on the orbital Hamiltonian for pristine graphene which, close to $K(K')$ points, is

$$\mathcal{H}_0 = \hbar v_F (\kappa \sigma_x k_x + \sigma_y k_y). \quad (1)$$

Here v_F is the Fermi velocity of graphene, k_x and k_y are the Cartesian components of the electron wave vector measured from $K(K')$, parameter $\kappa = 1(-1)$ for $K(K')$, and σ_x and σ_y are the pseudospin Pauli matrices acting on the two-dimensional vector space formed by the two triangular sublattices of graphene. Hamiltonian \mathcal{H}_0 de-

scribes gapless Dirac states with the conical dispersion $\varepsilon_0 = \nu \hbar v_F |\mathbf{k}|$ near the Dirac points; $\nu = 1(-1)$ for the conduction (valence) band.

The staggered potential describing the effective orbital energy difference on A and B sublattices of graphene on MoS_2 enters via the Hamiltonian,

$$\mathcal{H}_\Delta = \Delta \sigma_z s_0, \quad (2)$$

where σ_z is the pseudospin Pauli matrix and s_0 is the unit spin matrix; Δ is the proximity induced gap of the Dirac spectrum. Another consequence of the pseudospin inversion asymmetry is the sublattice-resolved intrinsic spin-orbit coupling. Indeed, the intrinsic coupling acts solely on a given sublattice: it is a next-nearest neighbor hopping [29]. We describe it in our model with parameters λ_I^A and λ_I^B for sublattices A and B , respectively. The corresponding proximity induced spin-orbit coupling Hamiltonian close to $K(K')$,

$$\mathcal{H}_{\text{SO}} = \lambda_I^A [(\sigma_z + \sigma_0)/2] \kappa s_z + \lambda_I^B [(\sigma_z - \sigma_0)/2] \kappa s_z, \quad (3)$$

is a generalization of the McClure-Yafet Hamiltonian for graphene [1, 30]. We denote by s_z the spin Pauli matrix, while by σ_0 the unit matrix acting on the pseudospin (sublattice) space. If $\lambda_I^A = \lambda_I^B$, the main effect of the intrinsic spin-orbit coupling is to enhance the anticrossing of the pristine graphene Dirac cones [28], leaving the

spin degeneracy intact. However, if $\lambda_I^A \neq \lambda_I^B$, as in our case, the spin degeneracy gets lifted by this intrinsic term already, reflecting the loss of space inversion symmetry.

Placing graphene on MoS_2 also breaks the lateral mirror symmetry, giving rise to the Rashba type spin-orbit coupling [29],

$$\mathcal{H}_R = \lambda_R (\kappa \sigma_x s_y - \sigma_y s_x), \quad (4)$$

where λ_R is the Rashba parameter and s_x, s_y are the spin Pauli matrices. In the hopping language, the Rashba coupling is the nearest-neighbor spin-flip hopping, contributing further to the spin splitting of the bands, and defining the spin quantization axis for each Bloch state, away from the time reversal points Γ and M .

Hamiltonian $\mathcal{H}_0 + \mathcal{H}_\Delta + \mathcal{H}_{\text{SO}} + \mathcal{H}_R$ fully describes graphene's bands at $K(K')$. Its eigenenergies are

$$\varepsilon_{\nu\mu} = \frac{1 + \nu\mu}{2} \left[\nu\Delta + \frac{1 + \nu}{2} \lambda_I^A + \frac{1 - \nu}{2} \lambda_I^B \right] - \frac{1 - \nu\mu}{4} \left[\lambda_I^A + \lambda_I^B - \nu \sqrt{(2\Delta - \lambda_I^A + \lambda_I^B)^2 + 16\lambda_R^2} \right], \quad (5)$$

where $\mu = 1(-1)$ for spin up (down) branches. The expectation values of the spin along z for the corresponding states are given by

$$\langle s_z \rangle_{\nu\mu} = \frac{\mu \kappa \hbar}{2} \left[\frac{1 + \nu\mu}{2} + \frac{1 - \nu\mu}{2} \frac{2\Delta - \lambda_I^A - \lambda_I^B}{\sqrt{(2\Delta - \lambda_I^A + \lambda_I^B)^2 + 16\lambda_R^2}} \right]. \quad (6)$$

Using the formulas for the eigenenergies, Eq.(5), and for the spin expectation values, Eq.(6), we can algebraically extract the orbital band gap Δ and the three spin-orbit parameters λ_I^A , λ_I^B , and λ_R by comparing to our first-principles data for the fine structure at K , see the inset to Fig. 1b). The extracted parameters are shown in Fig. 3 as a function of the applied transverse electric field. The orbital proximity gap Δ is about 0.5 meV in zero field. In fields greater than 0.5 V/nm, the gap exhibits a steep increase, which is related to the transfer of the electronic charge from graphene to MoS_2 , see Fig. 2. The proximity spin-orbit parameters in Fig. 3b) and c) are about 0.2 meV, which is 20 times more than in pristine graphene [28]. Similar giant values of spin-orbit coupling in graphene are induced by hydrogen adatoms [31–33], and even more by fluorine [34], though the mechanisms are different. Unlike in the adatom cases in which the induced spin-orbit coupling is only local, in our case the giant coupling is global. While the intrinsic

parameters λ_I^A and λ_I^B change rather moderately with applying the electric field, the Rashba parameter λ_R , see Fig. 3c), more than doubles in increasing the field from -2 to 2 V/nm.

What is the origin of the induced giant spin-orbit coupling in graphene on MoS_2 ? We trace the enhancement to the hybridization of the carbon orbitals with the d -orbitals of Mo. We find only 0.3% of d -orbitals at the K point by analyzing the calculated density of states. But when we turn the spin-orbit coupling on Mo atoms in the supercell off, the orbital gap in zero field remains almost unchanged ($\Delta = 0.506$ meV), while the spin-orbit parameters drop to their pristine graphene values $\lambda_I^A = 24 \mu\text{eV}$, $\lambda_I^B = 23 \mu\text{eV}$ and $\lambda_R = 10 \mu\text{eV}$, which are, curiously, also determined by d orbitals, but from carbon atoms [28].

Away from $K(K')$, the spin splittings depend on the momentum. In order to describe our first-principles data, we add the PIA (pseudospin inversion asymmetry) spin-orbit coupling term [32] which, like the intrinsic coupling,

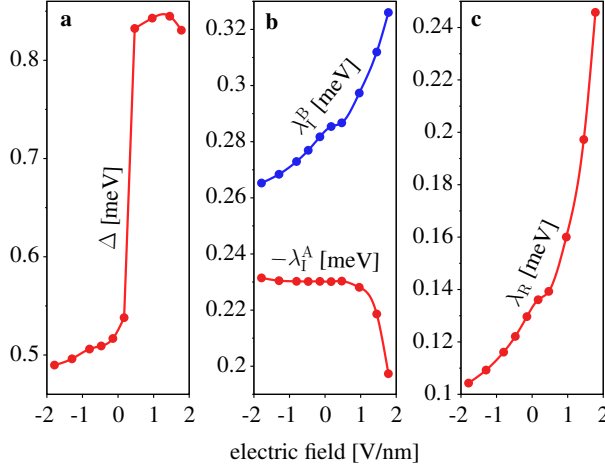


FIG. 3: Calculated effective Hamiltonian parameters at the K point: (a) hybridization gap Δ , (b) sublattice resolved intrinsic spin-orbit coupling λ_I^A and λ_I^B (they have opposite signs), and (c) Rashba parameter λ_R , as functions of the applied transverse electric field.

represents the next nearest neighbor hopping, but with a spin flip. The full model Hamiltonian describes the data perfectly, see Supplementary information.

Although our effective model should capture the basic physics of graphene on TMDC, the extracted parameters are for the specific supercell of graphene on MoS₂. Certainly, taking an even larger cell that could further reduce strain, or twisting the two layers as could happen in experiments, would lead to a different set of parameters, although the orders of magnitudes would likely stay. In a macroscopic experimental structure we expect Moire patterns which would transform our Hamiltonian into a Hamiltonian density, with an orbital gap and spin-orbit fields, perhaps even averaging some of the parameters (such as Δ and the difference between λ_I^A and λ_I^B) to zero. Our extracted parameters can then be viewed as effective standard deviations of the spatial variations, suitable as input for charge and spin transport model calculations for such samples. We also expect that graphene on TMDC could produce superlattice features as in graphene on hBN [35].

Optospintronics. We propose graphene-TMDC hybrids, such as the one studied above based on MoS₂, as an ideal platform for optospintronics. In Fig. 4a) we give an optical spin injection scheme into graphene. A circularly polarized light, tuned to the band gap of TMDC, excites electron spins by optical orientation [6, 36]. In effect, the light produces spin-polarized excitons which dissociate into spin-polarized electrons and holes. As in the recent optical experiment [24], we expect that electrons will be transferred to graphene, leaving holes behind in TMDC, although in which way electrons and holes split may depend on the TMDC material as well as on gating. The

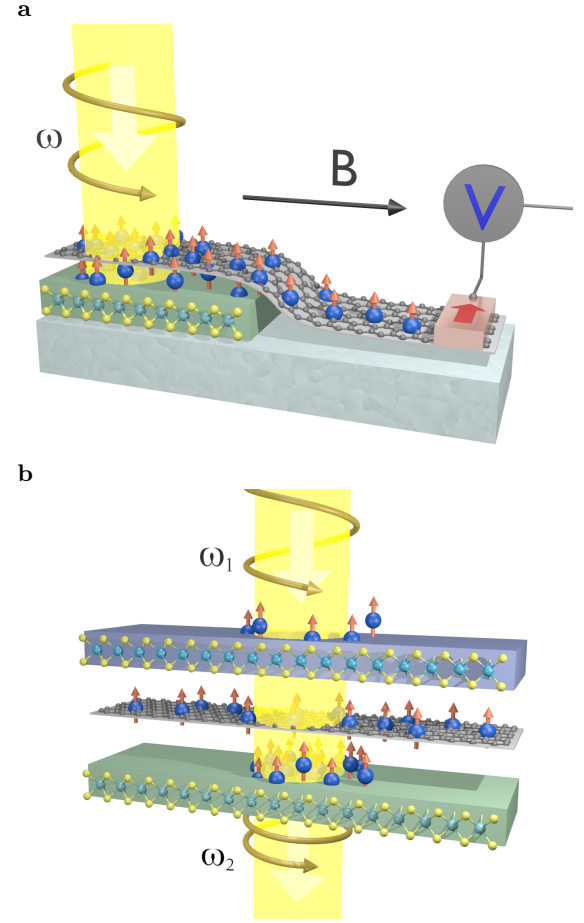


FIG. 4: Optospintronic schemes for graphene-TMDC hybrids. (a) Optical spin injection into graphene, facilitated by the semiconducting TMDC. A circularly polarized light excites spin-polarized electrons in the semiconductor. The spin is transferred to graphene where it can be detected as a Hanle signal by the ferromagnetic electrode. (b) Spin transfer between two different TMDCs, encapsulating graphene. Circularly polarized light tuned to the band gap of the top material excites electron spins which can tunnel to the lower material, exhibiting a circular luminescence peaked at its band gap frequency.

spin-polarized electrons (or holes) diffuse in graphene. One can detect this spin accumulation either optically, by observing a circular polarization of the photoluminescence [36] elsewhere in graphene on TMDC, or electrically. The latter is illustrated in Fig. 4a): a ferromagnetic electrode on top of graphene detects the presence of the spin accumulation in graphene [6, 7]. Spin precession in graphene can be observed as the Hanle signal (which is not possible to see in the spin-valley coupled TMDC [37]), by applying an external magnetic field transverse to the injected spin, providing Larmor precession [7].

Spin transport *per se* in graphene-TMDC bilayers should be fascinating. The presence of the giant, effectively uniform spin-orbit fields should give large spin Hall

signals, even greater than in hydrogenated graphene [33]. Most important, as our calculations show, the spin, like charge, properties of these structures are expected to be highly field tunable. The fascinating prospect of realizing the massive-massless electron gas coupling of the two electron gases, if the Fermi level is positioned in both band structures, calls for new theories of spin transport and spin relaxation in such hybrid systems.

To demonstrate spin tunneling from a TMDC through graphene one could use a sandwich structure, as pictured in Fig. 4b). The two semiconductors have different band gaps, allowing to discern the photoluminescence signals from the top and bottom layers. If the spin pumping light is tuned to the band gap of the top layer, the spin-polarized carriers would be excited there and tunnel through graphene to the bottom layer, in which they would recombine and emit circularly-polarized light with the frequency characteristics of the bottom material. One can envision influencing the signal with a transverse magnetic field, allowing for a Hanle effect. Another possibility is to measure the accumulated spin in the bottom layer using the magneto-optical Kerr effect, as in recent experiments on monolayer MoS₂ [38].

Conclusion. We have established by first-principles calculations a strong effect of MoS₂ on the spin properties of graphene, predicting a giant and field-tunable proximity spin-orbit coupling for Dirac electrons. We have introduced an effective spin-orbit Hamiltonian to describe the electronic states around the Fermi level, fitting perfectly the first-principles data. We have also showed that gating can tune the band offsets of the two layers, allowing to realize the unique system of coupled massless and massive electron gases. Finally, we have proposed to use graphene on TMDC as a platform for optospintronics with graphene-based two-dimensional materials structures.

We thank T. Korn, C. Schüller, C. Stampfer, B. Beschoten, T. Müller, and B. Özyilmaz for useful discussions and hints regarding possible experimental realizations of optospintronics with graphene-TMDC structures. This work was supported by DFG SFB 689, GRK 1570, and by the EU Seventh Framework Programme under Grant Agreement No. 604391 Graphene Flagship.

Supplementary information

Methods

Structural relaxation and electronic structure calculations were performed with Quantum ESPRESSO [39], using norm conserving pseudopotentials with kinetic energy cutoff of 60 Ry for wavefunctions. For the exchange-correlation potential we used generalized gradient approximation [40]. The supercell containing a 3×3 super-

cell of MoS₂ and 4×4 supercell of graphene was embedded in a slab geometry with vacuum of about 13 Å, with a dipole correction [41], which is crucial to get accurate band offsets between the Dirac point and the conduction band minimum of MoS₂. The resulting structure has a lattice mismatch of 2.8% which we split equally between graphene and MoS₂ by compressing graphene and stretching MoS₂ by 1.4%. The supercell has 59 atoms. The reduced Brillouin zone was sampled with 12×12 k points. Atomic positions were relaxed using the quasi-newton algorithm based on the trust radius procedure including the van der Waals interaction which was treated within a semiempirical approach [42, 43]. The calculated work function on the graphene side is 4.12 eV, while on MoS₂ it is 4.41 eV.

Spin eigenstates

The normalized eigenstates $\psi_{\nu\mu}$ at the K point of the Hamiltonian discussed in the manuscript in the basis $\sigma \otimes s = |A \uparrow, A \downarrow, B \uparrow, B \downarrow\rangle$ read

$$\begin{aligned} \psi_{+-} &= |0, i\alpha_+Q_+, 4\lambda_R\alpha_+, 0\rangle \simeq |A \downarrow\rangle, \\ \psi_{++} &= |1, 0, 0, 0\rangle = |A \uparrow\rangle, \\ \psi_{--} &= |0, 0, 0, 1\rangle = |B \downarrow\rangle, \\ \psi_{-+} &= |0, i\alpha_-Q_-, 4\lambda_R\alpha_-, 0\rangle \simeq |B \uparrow\rangle, \end{aligned} \quad (7)$$

where $\alpha_{\pm} = 1/\sqrt{16\lambda_R^2 + Q_{\pm}^2}$ and $Q_{\pm} = 2\Delta + \lambda_I^A + \lambda_I^B \pm \sqrt{(2\Delta + \lambda_I^A + \lambda_I^B)^2 + 16\lambda_R^2}$. The eigenvectors are ordered with increasing energy (using the extracted parameters): $\varepsilon_{+-} > \varepsilon_{++} > \varepsilon_{--} > \varepsilon_{-+}$. Analyzing the above eigenvectors we see that the valence bands are localized on sublattice B , while the conduction bands on sublattice A . The z component of the spin alternates from band to band. This behavior matches the first-principles results, see inset to Fig. 1b) in the manuscript. The top valence φ_{--} and bottom conduction φ_{++} states are pure pseudospin and spin states. On the other hand, spin-orbit coupling mixes spin and pseudospin of the outermost states. The eigenstates at K' have the same form, but opposite spins.

PIA coupling: spin splitting away from $K(K')$

To describe the calculated spin splittings away from K , we employ the PIA (short for pseudospin inversion asymmetry) spin-orbit term, introduced to study the effects of spin-orbit coupling in graphene due to hydrogen adatoms [32]:

$$\mathcal{H}_{\text{PIA}} = (\lambda_{\text{PIA}}^+ \sigma_z + \lambda_{\text{PIA}}^- \sigma_0)(k_x s_y - k_y s_x). \quad (8)$$

Here λ_{PIA}^+ and λ_{PIA}^- are the spin-orbit parameters representing the average, λ_{PIA}^+ , and differential, λ_{PIA}^- , PIA

coupling between the A and B sublattices. Like intrinsic spin-orbit coupling, PIA can be also represented by next-nearest-neighbor (same sublattice) hopping, but with a spin flip. The PIA terms turn the spin quantization axes of the electron states towards the graphene plane and add to the Rashba term for momenta away from the K point.

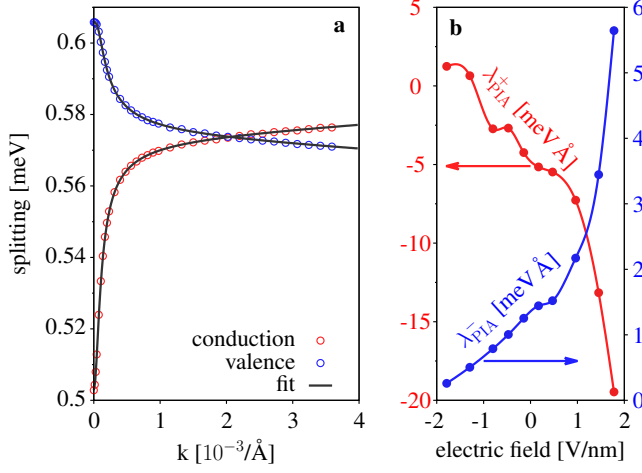


FIG. 5: Spin splitting away from K : emergence of PIA spin-orbit coupling in graphene on MoS_2 . (a) Spin splitting of conduction and valence bands from K ($k = 0$) in the direction towards Γ , at zero electric field. Solid lines are model fits, symbols are first-principles results. (b) Fitted PIA parameters at different transverse electric fields.

To obtain λ_{PIA}^+ and λ_{PIA}^- we add \mathcal{H}_{PIA} to the Hamiltonian $\mathcal{H}_0 + \mathcal{H}_{\Delta} + \mathcal{H}_{\text{SO}} + \mathcal{H}_{\text{R}}$, which is used directly at K in the manuscript, and fit to the first-principles data, keeping all other parameters as determined directly at K . In Fig. 5a we plot the calculated spin splittings of the valence and conduction bands. The full model, with PIA, fits the first-principles data perfectly. The fits are $\lambda_{\text{PIA}}^+ = -4.24 \text{ meV\AA}$, and $\lambda_{\text{PIA}}^- = 1.25 \text{ meV\AA}$. In Fig. 5b we plot the two PIA parameters as functions of the applied transverse electric field. Their tunability is enormous, much more than that of the Rashba hopping shown in the manuscript. As a final check we calculate, using the extracted parameters, the z components of the spin expectation values $\langle s_z \rangle$ in the vicinity of the K point for the low energy states. The model is fully consistent with the first-principles data, as seen in the comparison plotted in Fig. 6.

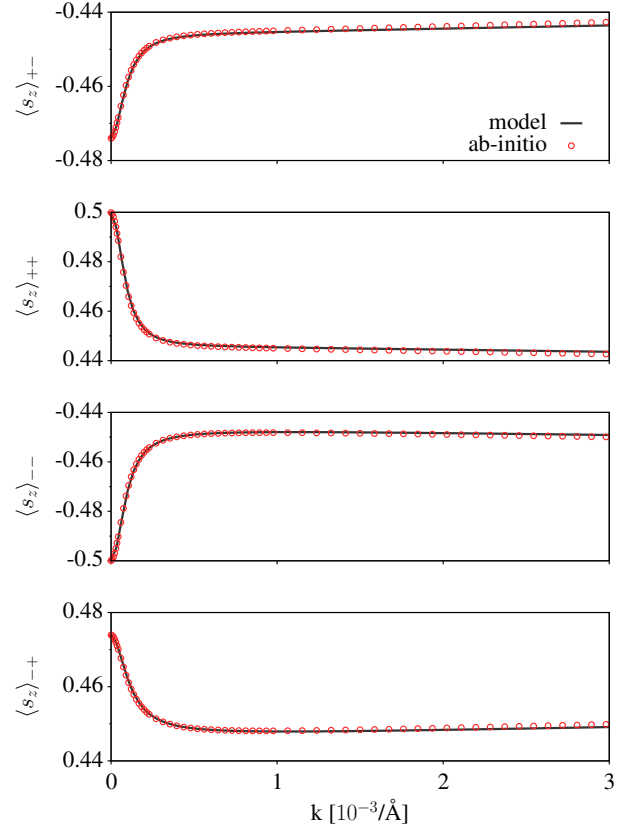


FIG. 6: Calculated spin expectation values for the four low energy bands in the vicinity of the K point for graphene on MoS_2 . Solid lines are model calculations and symbols are first-principles data.

[1] W. Han, R. K. Kawakami, M. Gmitra, J. Fabian, M. Gmitra, R. K. Kawakami, and W. Han, *Nature Nanotechnology* **9**, 794 (2014).
 [2] N. Tombros, C. Józsa, M. Popinciuc, H. T. Jonkman, and B. J. van Wees, *Nature* **448**, 571 (2007).

[3] K. Pi, W. Han, K. M. McCreary, A. G. Swartz, Y. Li, and R. K. Kawakami, *Phys. Rev. Lett.* **104**, 187201 (2010).
 [4] T.-Y. Yang, J. Balakrishnan, F. Volmer, A. Avsar, M. Jaiswal, J. Samm, S. R. Ali, A. Pachoud, M. Zeng, M. Popinciuc, et al., *Phys. Rev. Lett.* **107**, 047206 (2011).
 [5] K. F. Mak, C. Lee, J. Hone, J. Shan, and T. F. Heinz, *Phys. Rev. Lett.* **105**, 136805 (2010).
 [6] I. Žutić, J. Fabian, and S. Das Sarma, *Rev. Mod. Phys.* **76**, 323 (2004).
 [7] J. Fabian, A. Matos-Abiague, C. Ertler, P. Stano, and I. Žutić, *Acta Phys. Slovaca* **57**, 565 (2007).
 [8] O. Lopez-Sanchez, D. Lembke, M. Kayci, A. Radenovic, and A. Kis, *Nature Nanotechnology* **8**, 497 (2013).
 [9] C. Huang, S. Wu, A. M. Sanchez, J. J. P. Peters, R. Beanland, J. S. Ross, P. Rivera, W. Yao, D. H. Cobden, and X. Xu, *Nature Materials* **13**, 1096 (2014).
 [10] C.-H. Lee, G.-H. Lee, A. M. van der Zande, W. Chen, Y. Li, M. Han, X. Cui, G. Arefe, C. Nuckolls, T. F. Heinz, et al., *Nature Nanotechnology* **9**, 676 (2014).
 [11] A. Pospischil, M. M. Furchi, and T. Mueller, *Nature Nanotechnology* **9**, 257 (2014).
 [12] A. Kormányos, G. Burkard, M. Gmitra, J. Fabian, V. Zólyomi, N. D. Drummond, and V. Fal'ko, *2D Materials* **2**, 022001 (2015).
 [13] D. Xiao, G.-B. Liu, W. Feng, X. Xu, and W. Yao, *Phys.*

- Rev. Lett. **108**, 196802 (2012).
- [14] K. F. Mak, K. He, J. Shan, and T. F. Heinz, *Nature Nanotechnology* **7**, 494 (2012).
 - [15] H. Zeng, J. Dai, W. Yao, D. Xiao, and X. Cui, *Nature Nanotechnology* **7**, 490 (2012).
 - [16] Y.-C. Lin, N. Lu, N. Perea-Lopez, J. Li, Z. Lin, X. Peng, C. H. Lee, C. Sun, L. Calderin, P. N. Browning, et al., *ACS Nano* **8**, 3715 (2014).
 - [17] M.-Y. Lin, C.-E. Chang, C.-H. Wang, C.-F. Su, C. Chen, S.-C. Lee, and S.-Y. Lin, *Appl. Phys. Lett.* **105**, 073501 (2014).
 - [18] A. Azizi, S. Eichfeld, G. Geschwind, K. Zhang, B. Jiang, D. Mukherjee, L. Hossain, A. F. Piasecki, B. Kabijs, J. A. Robinson, et al., *ACS Nano* **9**, 4882 (2015).
 - [19] C.-P. Lu, G. Li, K. Watanabe, T. Taniguchi, and E. Andrei, *Phys. Rev. Lett.* **113**, 156804 (2014).
 - [20] H. Coy Diaz, J. Avila, C. Chen, R. Addou, M. C. Asensio, and M. Batzill, *Nano Letters* **15**, 1135 (2015).
 - [21] N. A. Kumar, M. A. Dar, R. Gul, and J. Baek, *Materials Today* **18**, 286 (2015).
 - [22] S. Bertolazzi, D. Krasnozhon, and A. Kis, *ACS Nano* **7**, 3246 (2013).
 - [23] W. Zhang, C.-P. Chuu, J.-K. Huang, C.-H. Chen, M.-L. Tsai, Y.-H. Chang, C.-T. Liang, Y.-Z. Chen, Y.-L. Chueh, J.-H. He, et al., *Sci. Rep.* **4** (2014).
 - [24] K. Roy, M. Padmanabhan, S. Goswami, T. P. Sai, G. Ramalingam, S. Raghavan, and A. Ghosh, *Nature Nanotechnology* **8**, 826 (2013).
 - [25] A. Avsar, J. Y. Tan, T. Taychatanapat, J. Balakrishnan, G. K. W. Koon, Y. Yeo, J. Lahiri, A. Carvalho, A. S. Rodin, E. C. T. O'Farrell, et al., *Nature Communications* **5** (2014).
 - [26] J. Hohenberg and W. Kohn, *Phys. Rev.* **136**, B864 (1964).
 - [27] B. Scharf and A. Matos-Abiad, *Phys. Rev. B* **86**, 115425 (2012).
 - [28] M. Gmitra, S. Konschuh, C. Ertler, C. Ambrosch-Draxl, and J. Fabian, *Phys. Rev. B* **80**, 235431 (2009).
 - [29] S. Konschuh, M. Gmitra, and J. Fabian, *Phys. Rev. B* **82**, 245412 (2010).
 - [30] J. W. McClure and Y. Yafet, in *Proceedings of the 5th conference on carbon* (Pergamon Press, 1962), vol. 1, pp. 22–28.
 - [31] A. H. C. Neto and F. Guinea, *Phys. Rev. Lett.* **103**, 026804 (2009).
 - [32] M. Gmitra, D. Kochan, and J. Fabian, *Phys. Rev. Lett.* **110**, 246602 (2013).
 - [33] J. Balakrishnan, G. Kok, W. Koon, M. Jaiswal, and A. H. C. Neto, *Nature Physics* **9**, 1 (2013).
 - [34] S. Irmer, T. Frank, S. Putz, M. Gmitra, D. Kochan, and J. Fabian, *Phys. Rev. B* **91**, 115141 (2015).
 - [35] R. V. Gorbachev, J. C. W. Song, G. L. Yu, A. V. Kretinin, F. Withers, Y. Cao, A. Mishchenko, I. V. Grigorieva, K. S. Novoselov, L. S. Levitov, et al., *2D Materials* **346**, 448 (2014).
 - [36] F. Meier and B. P. Z. (Eds.), *Optical Orientation* (North-Holland, New York, 1984).
 - [37] G. Sallen, L. Bouet, X. Marie, G. Wang, C. R. Zhu, W. P. Han, Y. Lu, P. H. Tan, T. Amand, B. L. Liu, et al., *Phys. Rev. B* **86**, 081301 (2012).
 - [38] G. Plechinger, P. Nagler, Schüller, and T. Korn, arXiv:1404.7674 (2014).
 - [39] P. Giannozzi and et al., *J. Phys.: Condens. Matter* **21**, 395502 (2009).
 - [40] J. P. Perdew, K. Burke, and M. Ernzerhof, *Phys. Rev. Lett.* **77**, 3865 (1996).
 - [41] L. Bengtsson, *Phys. Rev. B* **59**, 12301 (1999).
 - [42] S. Grimme, *J. Comput. Chem.* **27**, 1787 (2006).
 - [43] V. Barone, M. Casarin, D. Forrer, M. Pavone, M. Sami, and Vittadini, *J. Comput. Chem.* **30**, 934 (2009).